3

Mechanisms of Plastic Deformation in AZ31 Magnesium Alloy Investigated by Acoustic Emission and Electron Microscopy

Miloš Janeček and František Chmelík
Charles University Prague, Department of Physics of Materials
Czech Republic

1. Introduction

Magnesium alloys are the lightest metallic structural materials and are therefore very attractive in applications in automobile, railway and aerospace industries where the mass reduction is an important issue. However, owing to their hexagonal close-packed structure and a limited number of slip systems, Mg alloys exhibit only limited ductility and accommodation ability. Parts of these alloys for structural applications are often produced by casting with no or very limited mechanical pressing. This obviously limits the range of possible engineering applications of Mg alloys.

In the recent years, there has been a renewed interest in Mg alloy sheet products, especially in automotive applications where considerable weight savings can be made by substituting magnesium for aluminium or steel components. Mg-3Al-1Zn alloy (AZ31) is currently the most common Mg alloy used for sheet applications. Due to its poor cold rolling response it has to be rolled at elevated temperatures, which considerably increases manufacturing costs of sheet products of this alloy. Optimization of conditions of the hot rolling process is therefore a big challenge. The properties of the rolled sheet obviously depend on the initial state of the material, the temperature of plate before rolling and many other parameters. However, at present there is only a limited knowledge of this area. One of the possible ways how to improve the final properties of the rolled state is to optimize the conditions of the material preheating before rolling. Too high temperature of preheating increases the costs of the final sheet and too low temperature may result in the failure of the material during successive rolling.

Next to rolling the techniques of severe plastic deformation attracted recently the interest of researchers. Ultrafine-grained materials processed by these techniques exhibit enhanced mechanical and other physical properties and offer a wide range of possible practical applications. The properties of materials with fine grain sizes and face centred cubic lattice were extensively studied and reported in the literature. On the other hand, there is a limited knowledge of properties and microstructure evolution of materials with hexagonal structure. AZ31 alloy is a typical representative of this class of materials.

A well established method of investigating the dynamic processes taking place during plastic deformation is acoustic emission (AE). AE signals originate from transient elastic waves, which are generated within the material due to sudden localized structural changes. Typical sources of intense AE are collective dislocation movement or twinning.

The objective of this review paper is to investigate various mechanisms of plastic deformation in AZ31 magnesium alloy by AE and to correlate them with the evolution of microstructure observed by electron microscopy and electron diffraction and to asses critically the differences in the material processed by different processing routes.

2. Experimental part

2.1 Experimental material

In this chapter the properties of AZ31 (3 wt.% Al, 0.8 wt.%Zn, 0.2 wt.% Mn) alloy as a typical representative of wrought magnesium alloys are summarized. Two different processing routes, in particular

a. hot rolling,
b. severe plastic deformation,

were used to prepare the material for the investigation. Squeeze cast material was used as a reference material to compare the behaviour of wrought and cast AZ31.

The properties of the material were investigated by different experimental techniques.

Mechanical properties in tension and compression were investigated by standard screw driven Instron and Zwick machines equipped with furnaces allowing deformation up to 300°C. Fatigue behaviour was investigated both in push-pull and rotating beam tests up to the very high cycle range.

During mechanical tests (tension, compression, fatigue) AE was monitored using a sophisticated new generation AE system whose details will be described in the following part as its application to detect and understand microphysical processes occurring during plastic deformation, fatigue and fracture is one of the main topics of this paper.

Microstructure evolution and characterization was performed using various techniques of electron microscopy and electron diffraction – light, scanning and transmission electron microscopy, electron back scattered diffraction. These techniques are particularly important in the characterization of ultrafine-grained materials prepared by severe plastic deformation. X-ray diffraction was also used to investigate microstructure and texture evolution in various specimens.

2.2 Acoustic emission

2.2.1 Introduction

AE may be characterized as a manifestation of transient elastic waves arising in a material from sudden localized irreversible structure changes. Since the pioneering work of Kaiser (Kaiser, 1953), AE has been frequently used to investigate plastic deformation of materials. AE methods that were used in the past and reported in the literature both by other authors (Botten, R. et al., 2001; Vinogradov et al., 2003) and in our previous work (Richeton et al., 2006; Mathis et al., 2006), were based on evaluation of individual AE events which surpass some set threshold level. Various parameters of such events can be evaluated such as frequency of events for different thresholds, energy of events and waveforms of AE signal. Nevertheless, in many cases the effects remain hidden below the minimum threshold given by the noise level of the equipment. In such cases AE methods did not allow detecting any events and as such could not contribute to the understanding of processes in the material. In our laboratory we have developed a qualitatively new approach to the AE measurement, which in some extent eliminates the above described limitations (Král et al. 2007). The main difference from previously used methods is a continuous sampling and storage of the AE

signal from several channels as measured by the AE transducer and performing consequently a statistical analysis on a complete stored signal data. The fact that the complete signal is stored allows to i) run various successive analyses, ii) evaluate individual time moments with respect to the properties of the entire signal set, iii) use time consuming analyses that would not be possible to use in real time (during experiment).

2.2 Principles and systems of acoustic emission detection

The detection of AE is based on its physical nature, namely the elastic energy release due to some irreversible change of (micro)structure. Near the source of AE the released energy (AE event) forms the stress pulse, which propagates through the material bulk as transient elastic waves and at the surface of the material it is transformed into a certain wave mode which corresponds to the geometrical configuration and the dimensions of the specimen. The wave component perpendicular to the surface may be detected by piezoelectric transducers, which are coupled to the specimen surface either mechanically or through a waveguide. Electrical signal from the transducer (emission signal) is first preamplified and then led to the input of the measuring system, where it is amplified and analyzed.

The AE signal is either of continuous character, whereby the amplitude does not fall under a certain threshold level during relatively long period of time, or discontinuous. The former has a character of noise while the latter features pulses, distinctly separated in time, so called emission events.

In case of the continuous AE the mean quadratic value of the signal voltage and the number of hits above threshold levels are evaluated during a certain adjustable period of time. In case of discontinuous AE each emission event is evaluated independently. The following parameters are usually used to characterize individual separated events, see Fig. 1:

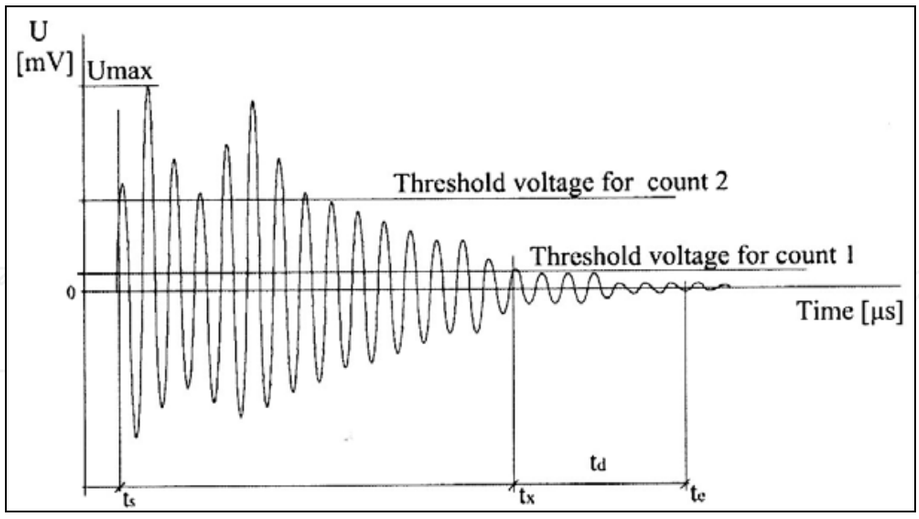

Fig. 1. The characteristics of a single AE event at the threshold level 1

- t_s is the onset of AE event when the first signal overshoot above the threshold level is detected,
- t_d is the event dead time,
- t_x is the time when the last overshoot is detected,
- t_e is the termination of the event ($t_e = t_x + t_d$),

- t_e-t_s is the duration of the event.

Two different systems of AE detection may be employed:

a) a standard generation of AE systems (we use the system DAKEL-XEDO-3 by the manufacturer DAKEL-ZD Rpety, Czech Republic). In this case the electrical signal is analyzed and evaluated in real time and the evaluated data (AE parameters) are stored. A two threshold level detection giving a simple amplitude discrimination and two AE count rates (AE1 and AE2) is used and the sampling rate of 4 MHz is used.

b) a new generation DAKEL-CONTI-4 AE system allows continuous sampling and storage of AE signal from 1 up to 4 channels with 2 MHz sampling frequency. The sampled AE signal is continuously stored on a dedicated hard disk connected to the measuring unit via a high speed interface, i.e. no data processing by the computer used to control the measuring unit takes place and high data transfer speed is ensured. The software enables both the evaluation of individual AE events in a standard way (Trojanová & Cáceres, 2007) (two-threshold-level detection recommended by an ASTM standard (ASTM, 1994) was used with the thresholds set to 1.06 and 2.10 mV) and the analysis of the complete stored spectra based on statistical method. The method of averaged frequency spectra was used. A miniaturized MICRO-06 piezoelectric transducer with 3 mm diameter and a flat response in a frequency band from 100 to 600 kHz was used. If we denote generally the registered AE signal in time t as $x(t)$ then the total energy E in some time interval can be written as

$$E = k \int x^2 (t)\, dt, \tag{1}$$

where k is a constant equal to Z^{-1}, where Z is the impedance of the experimental set-up. In the case of discrete substitution the integral in (1) is replaced by a sum and dt is replaced by f^{-1}, f being the sampling frequency, which yields

$$E = Z^{-1} f^{-1} \sum x_i^2 \tag{2}$$

By confining to relative values of energy, the factors Z^{-1} and f^{-1} in (2) are insignificant. The value of the sum must be determined and related to some unit value (typically the maximum value registered during the experiment). The sum in (2) is computed in time intervals $t_n = n \cdot 4096$ μs for 8192 samples (which corresponds to 4096 μs at the sampling frequency of 2 MHz).

The 4096 μs interval was found to be optimal with the respect to noise minimization while preserving sufficient sensitivity for detecting effects in AE signal.

The energy E_k of the k-th interval of 4096 μs may be expressed as (k is going from 0):

$$E_k = K \sum_{i=kx8192}^{(k+1)x8192} x_i^2 , \tag{3}$$

where K is a constant found from the condition $\{E_k\} = 1$. Histograms of relative energies of AE signal are then computed in 10 s time intervals, i.e. each histogram comprises 2441 energies.

3. Results and discussion

3.1 Hot rolled AZ31

Wrought magnesium alloys have a high potential for structural application due to their improved mechanical properties compared to cast components.

However, due to the hexagonal close-packed (hcp) crystallographic structure, a limited activation of slip planes at room temperature is available so the formability of the sheet is poor. Furthermore, the mechanical properties show an anisotropic behaviour (Kaiser et al. 2003). It was also found that the heat treatment condition has an influence on the extension of the anisotropic behaviour. Thus, a heat treatment of the stress-relieved sheet leads to changes in the microstructure as well as in the texture of the material and therefore results in a decrease of the orientation dependence of mechanical properties.

Basal slip is known to be the most important mechanism of plastic deformation in magnesium (Emley, 1996). However, there are only three equivalent basal slip systems in Mg, but the compatibility of deformation in polycrystals requires at least five independent slip systems. Therefore, secondary (prismatic, pyramidal) slip systems or twinning, primarily in (10.2) planes, must be activated during deformation. Furthermore, twinning in Mg can reorientate basal planes so that they become more favourable oriented for slip (Zhang et al., 2000). The activation of twinning itself depends on grain orientation (Emley, 1996).

AE, which stems from transient elastic waves, generated within a material due to sudden localised and irreversible structure changes, responds to dislocation motion and twinning (Heiple, & Carpenter, 1987) and therefore yields information on the dynamic processes involved in plastic deformation of magnesium alloys. Friesel and Carpenter (Friesel & Carpenter, 1984) investigated AE during the deformation of pure Mg and an AZ31B alloy and found a distinct correlation of the AE activity with sample orientation, purity, strain rate and the mode of testing (tension, compression).

In our previous investigation (Bohlen et al., 2004) AE was observed and analysed during plastic deformation of an AZ31 rolled sheet in an H24 temper as well as after a heat-treatment at elevated temperatures. The AE count rates showed a well-known correlation with the stress–strain curves revealing a well-defined peak close to the macroscopic yield point followed by a subsequent decrease in the AE activity.

In all cases, deformation twinning and dislocation glide were found to be the major sources of AE. AE proves therefore for a justifiable method to study dynamic processes involved in plastic deformation of magnesium and magnesium alloys.

One of the effects that can contribute to the understanding of deformation mechanisms is a spatio-temporal localization of plastic deformation (Portevin–Le Chatelier effect, hereafter PLC effect) that occurs in some alloys at suitable deformation conditions. In hexagonal alloys, an interplay of the PLC effect with twinning (non-propagative plastic instability) may be anticipated. (Caceres et al., 2002) observed recently the PLC effect in a heat-treated AZ91 alloy deformed at room temperature. However, to date no PLC effect was reported in AZ31 alloy (Tan & Tan, (2002). Therefore we employed AE to investigate unstable plastic flow in a hot-rolled AZ31 alloy under different deformation conditions.

The extruded AZ31 alloy was hot rolled at 300°C by twelve successive passes perpendicular to the extrusion direction. The thickness reduction between individual passes of rolling was kept constant. The final thickness after the reduction was 1 mm. The stripes were compact with limited cracking on both sides of the rolled stripe and had a width of 40 to 43 mm and the length of 950 to 1100 mm. Two sets of samples prepared from hot-rolled sheets, which were preheated at two different temperatures, T_{PR} (325 and 475°C) prior to individual passes of hot rolling were studied. AE study of the unstable plastic flow under different deformation conditions (temperature, strain rate) was performed. In Fig. 2, the true stress–true strain curves for the highest (200°C) and lowest test temperatures (RT) and both specimens are shown. The deformation behaviour differs significantly at both temperatures.

While at RT the flow stress increases with increasing deformation up to the fracture, at the temperature of 200°C the strain hardening region is limited to a small region of low strains only and is followed by an extended softening region for larger strains. Both the yield stress and the tensile strength decrease with increasing temperature of deformation. The ductility was found to increase significantly with increasing temperature of deformation in both specimens. At both temperatures of deformation enhanced ductility was also observed in the specimen preheated at higher temperature. The PLC effect was observed for all used strain rates both at room and elevated temperatures. Plastic deformation is accompanied by a pronounced AE activity with a maximum near the yield point. With further straining AE activity decreases significantly. However, some AE persists to fracture. Fig. 3 shows an example of a stress–strain curve correlated with the AE counts at room temperature. The stress is plotted as a solid line and the AE counts as bars.

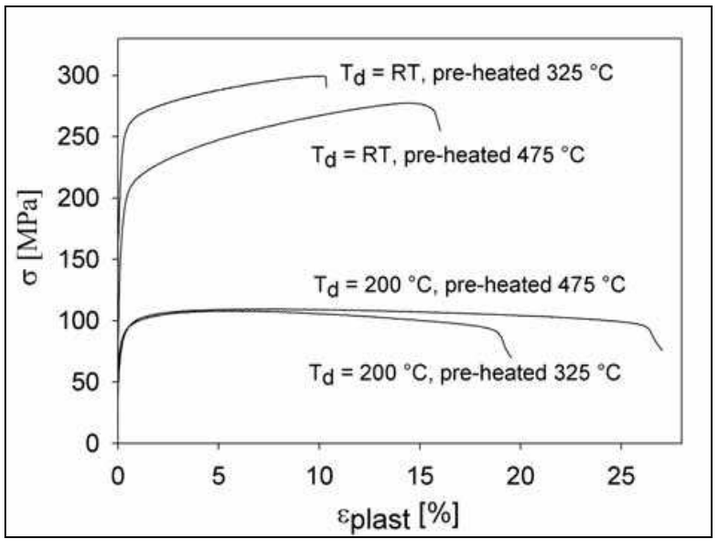

Fig. 2. Stress–strain curves for two AZ31 specimens deformed at RT and 200°C; T_d= deformation temperature.

The AE counts reveal a well-defined master curve with superimposed large bursts. The burst character of AE is clearly seen in the inset of Fig. 3, where a small portion of serrated stress–strain curve correlated with the AE counts is shown. Such an AE response is typical for the PLC effect, see, e.g. (Chmelík et al., 2002). The AE counts show a similar shape at both threshold levels, which indicates that no changes in the AE count distribution occur throughout the tests.

The shape of the AE count rate dependences does not seem to be influenced by the deformation conditions as the respective curves for all tested temperatures and strain rates have a similar shape. Therefore, only two examples of AE curves are shown, for RT in Fig. 3 and 200°C in Fig. 4. However, two differences are worth noting. Firstly, the AE activity increases with increasing temperature of preheating, and secondly, a distinct double peak at the yield point is observed at 200°C, see Fig. 4, while only a single AE peak curve was found at RT, see Fig. 3.

The microstructure of the alloy was investigated by light and transmission electron microscopy. The average grain size of the as extruded alloy is 200-300 μm. Hot rolling causes significant grain refinement. The bimodal distribution of grains was found in hot

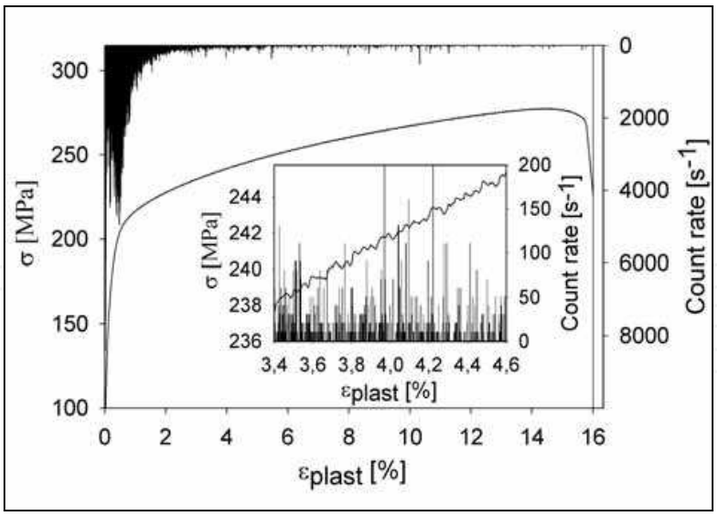

Fig. 3. A typical stress–strain curve and the corresponding AE count rates (the character of serrations and AE bursts are shown in the inset). The *y*-axis for the AE plot is on the right hand side of the graph and has an inverse polarity, i.e. the bars corresponding to AE counts are plotted from the upper border of the graph downwards.

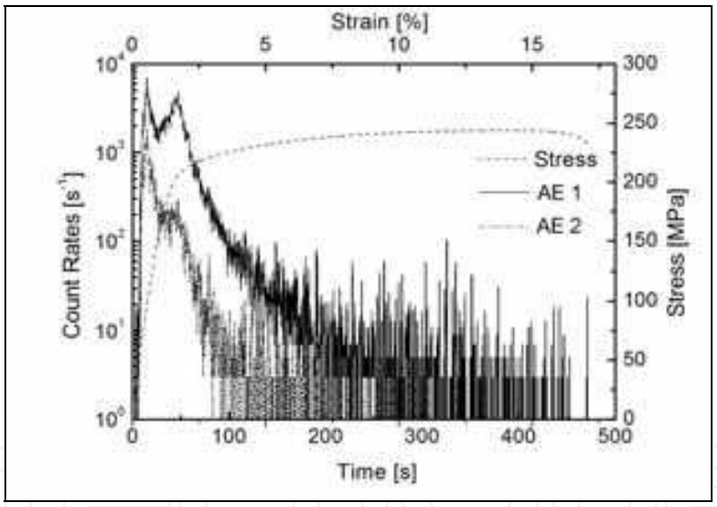

Fig. 4. The AE curve of AZ31 alloy deformed at 200°C showing a double peak at the yield point (AE 1 and AE 2 are count rates at the respective threshold levels 1 and 2, strain rate = 3.3×10^{-4} s^{-1}).

rolled sheets. The preheating temperature between individual steps of rolling influences the final grain size. The average size of the finer population of grains in the alloy preheated at 325°C and 475°C is 9 μm and 17 μm, respectively, whereas that of the bigger grains is 33 μm and 71 μm, respectively.

Fig. 5 illustrates an example of the microstructure of specimens deformed at RT and 200°C to 2.8%. Extensive twinning was found almost in all areas of the specimen implying that twinning is prevalent mechanism of deformation at low strains. Several families of almost parallel twins with high density of dislocations passing through several grains and

intersecting each other were observed (so called compound twinning (Yin et al., (2005)). Much higher number of twins was found in the specimen deformed at RT (Fig. 5a) than in that deformed at 200°C (Fig. 5b).

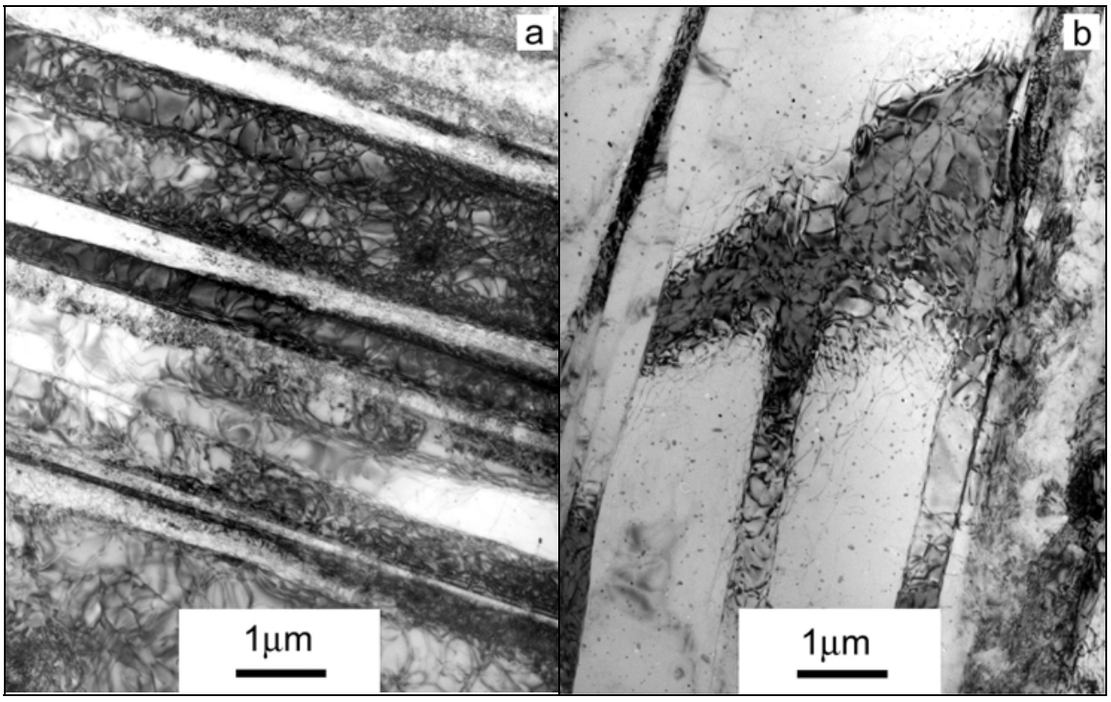

Fig. 5. Twinning in deformed AZ31 a) RT, b) 200°C (ε = 2.8%, T_{PR} = 475°C)

Serrated flow has been recently observed in an AZ91 alloy at room temperature by Corby (Corby et al, 2004). The authors discuss the possible mechanisms controlling plastic instabilities in this alloy suggesting some combined effect of both solutes - Al and Zn. The same mechanisms are probably in effect in the AZ31 alloy. Even lower concentrations of Al in AZ31 alloy as compared to AZ91 are high enough to ensure its role in the PLC effect formation. On the other hand, the concentration of Zn is the same in both alloys and therefore its enhancing effect on prismatic slip and consequently the forest dislocation formation remains unchanged in AZ31.

3.2 Ultra-fine grained AZ31

3.2.1 Mechanical properties and acoustic emission

Several techniques of severe plastic deformation were shown to result in significant grain refinement of coarse-grained polycrystals. Over recent years, equal channel angular pressing (ECAP) became one of the most popular methods of severe plastic deformation for producing bulk ultra-fine grained (UFG) metallic materials. This method leads to grain refinement due to shear deformation introduced into a work piece which is repeatedly pressed through an angular channel without changing its cross-sectional dimensions (Segal, 1995). Generally, this leads to improved mechanical properties, such as high strength and, at proper processing conditions, also to reasonable room temperature ductility (Valiev et al., 2000). At elevated temperatures, high strain rate superplastic behaviour can be achieved due to ECAP processing (Watanabe et al., 2003; Matsubara et al., 2003). Magnesium alloys with

their low density and high specific strength are of interest for many technical applications especially in the field of automotive industry. There is a strong demand to improve the mechanical properties of these materials to broaden their field of application. Depending on the targeted application, either a good combination of strength and ductility or a good superplastic formability is sought. Beneficial effects of ECAP on magnesium alloys have been demonstrated recently by many authors, e.g. (Mabuchi et al, 1997; Kim et al., 2003; Yoshida et al., 2004). Various ECAP conditions were also investigated. Grain refinement and deformation twins after ECAP processing in the temperature range of 200–250°C were observed (Kamado et al., 2000; Mukai et al, 2001; Agnew et al., 2001). Furthermore, recrystallisation was found to occur above 200°C by Kamado et al. (Kamado et al., 2000). Average grain size of 1μm after eight passes of ECAP by route B_C at 200°C was reported in (Mukai et al, 2001). Agnew (Agnew et al., 2001) conducted ECAP of AZ31 at 300°C because they experienced cracking of samples at a low temperature of 200°C. They neither found any significant grain refinement nor a change in the tensile properties at 300°C.

For ECAP processing of Mg alloys with their hcp crystal structure, elevated pressing temperatures are necessary to activate a sufficient number of slip systems (Ishikawa et al., 2005). To avoid excessive dynamic recrystallization during ECAP, the processing temperature should be chosen carefully, however.

AE from the magnesium alloy AZ31B alloy was first investigated by (Friesel & Carpenter, 1984). In their investigation dislocation glide and deformation twinning were identified as main sources of AE. Due to the lack of experimental data on AE in UFG Mg alloys we performed a detail investigation of the AE behaviour of ECAP processed AZ31 at different temperatures in compression tests and compare these results with those for the material that did not undergo the ECAP processing.

A squeeze-cast magnesium alloy AZ31 having an initial grain size of approximately 450μm was used as the initial material. The specimens after one and four passes of ECAP were used in this investigation and compared with the as squeeze-cast material. ECAP was performed at 200°C following route B_C and the pressing speed of 15 mm/min was used.

Compression tests at a strain rate of 10^{-3} s^{-1} on specimens of ECAP processed material and the reference, not pre-strained material, were performed on an Instron 4507 universal testing machine at room temperature as well as at 200°C and 300°C. The hardening behaviour for the ECAP processed and the as cast material was also evaluated from true stress versus true strain curves at different temperatures. Except for room temperature tests of the ECAP processed specimens, the strain hardening coefficient was determined up to a true strain of 0.1. As early buckling was observed in ECAP processed AZ31 in room temperature tests, only true strains up to approximately 0.02–0.03 depending on the specimen behaviour were used to determine the strain hardening coefficient.

AE was measured during compression testing. As the transducer could not withstand high temperatures, it was not possible to measure AE inside the furnace for the tests at 200°C and 300°C. Therefore, as a general setup, a waveguide was used to route the signals to the transducer that was fixed outside the furnace. After preamplification, the AE signal was analysed with the Dakel XEDO-3 AE system.

Microstructure evolution with strain due to ECAP and after the compression deformation at various temperatures was observed by TEM.

After ECAP an inhomogeneous structure was found. The typical microstructure after one pass of ECAP is presented on the TEM micrograph in Fig. 6. It is a typical heavily deformed structure with high density of homogeneously distributed dislocations, cf. Fig. 6a. Several

bands of parallel elongated subgrains passing through the whole transparent area of the thin foil were also found in the specimen, cf. Fig. 6b. With further pressing the first grains having sharp boundaries and high misorientation started to be formed. However, the grain structures were not homogeneous. Rather, a mixed structure of coarse and fine grains was observed. Figure 7 shows an example of such a zone with grains. Some grains contained no dislocations whereas in others dislocations were clearly seen. The presence of dislocations in some recrystallized grains is probably due to large strain imposed by ECAP. The average size of bigger grains was 1-3 μm, while that of smaller grains varied from 500 to 800 nm. Fine grains of 100 nm were also found in the specimen. Besides zones with clearly formed grains, which were observed in approximately 80% of the transparent areas of the specimen, the specimen contained regions of heavily deformed structure similar to that after one pass of ECAP.

Microstructure changes due to deformation are presented only for the highest temperature (300°C). TEM micrographs of both specimens (after 1 and 4 passes of ECAP) are presented in Fig. 8. In order to demonstrate the influence of temperature, all specimens were deformed to the same level of compressive strain of approximately 1%. It is clearly seen that dynamic recrystallization occurs during the compression test. However, the final microstructure is rather inhomogeneous with respect to the direction of ECAP pressing before straining. A clear influence of strain imposed by ECAP pressing is also seen. Figure 8a presents the microstructure of the specimen after 1 pass taken from the cross-section plane (X). Deformed structure with high density of heterogeneously distributed dislocations was observed in this specimen. Dislocation or cell wall formation was often observed. Only very few recrystallized grains were found in this specimen. By contrast, in the deformed specimen after 4 passes of ECAP only recrystallized grains of the average size of several micrometers

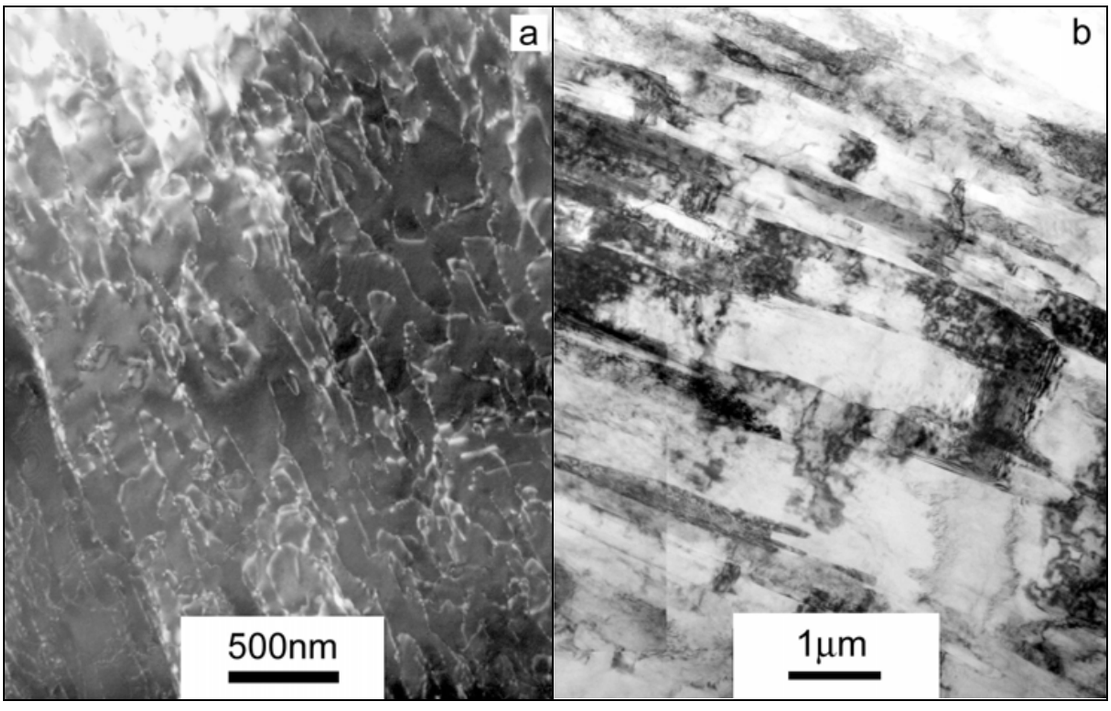

Fig. 6. The microstructure of AZ31 alloy after 1 pass of ECAP (X plane), a) dislocations – Weak beam dark field , B=[1-2.0], g=(-10.1), b) subgrains, B=[1-2.0], g=(10.0]

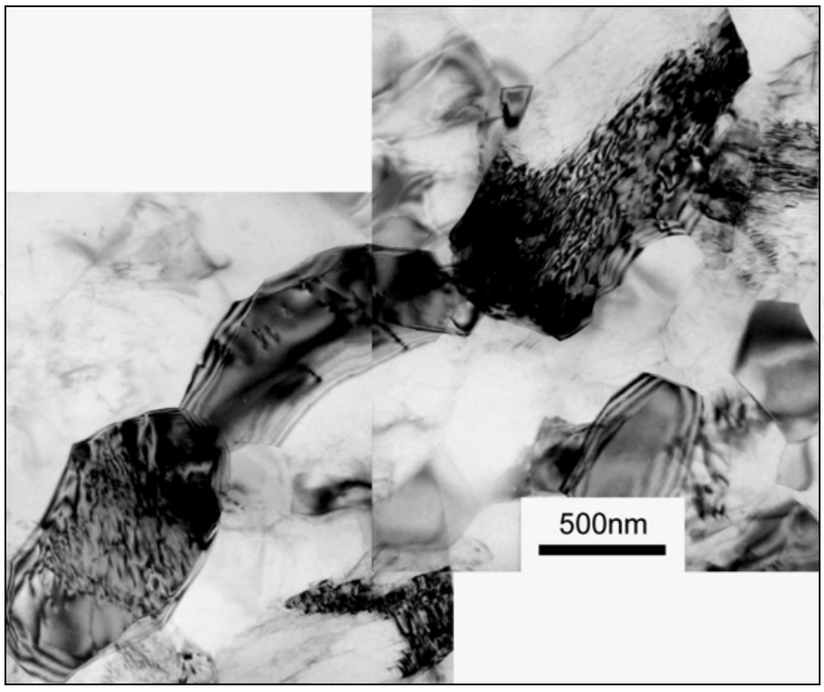

Fig. 7. TEM micrograph of the specimen after 4 passes of ECAP

were observed, as seen in Fig. 8b. The size of several grains (not shown in the micrograph) even exceeded 10 μm. Some grains contained dislocations, while others did not. The heterogeneity of the deformed structure of the specimen after 1 pass of ECAP is obvious from the micrographs in Figs. 8a and 8c. Figure 8c shows the microstructure of this specimen in the longitudinal plane (Y). The microstructure consists of recrystallized grains of the average size of approximately 1 μm with some dislocations within the grains. By contrast, no significant heterogeneity of the microstructure was found in the deformed specimen after 4 passes of ECAP. In Fig. 8d the microstructure of the deformed specimen in the longitudinal plane is shown. Fully recrystallized structure very similar to that in the cross-section plane is seen. The average size of dynamically recrystallized grains increases with increasing strain imposed by ECAP.

Mechanical properties during compression tests are presented in Fig. 9. It shows the temperature dependence of the yield stress of an as cast specimen and the specimens after 1 and 4 passes of ECAP. ECAP pressing resulted in significant increase of the yield stress as measured by compression tests. The as-received alloy (after squeeze-casting, marked 0P) deformed at room temperature (RT) had a yield stress of 65 MPa. After 1 ECAP pass the yield stress increased to 120 MPa whereas after 4 passes the yield stress reached 210 MPa, which is about three times larger than that of the as cast specimen and twice as large as that for the specimen after 1 ECAP pass. Two temperature regions were found in the as cast specimen and the specimen after one ECAP pass. In the low temperature region ($T < 200°C$) the yield stress was almost independent of the temperature or decreased only slightly with the temperature. At higher temperatures ($T>200°C$) the yield stress decreased with increasing temperature. In the specimen after 4 passes of ECAP the yield stress decreased with increasing temperature in the whole temperature region at a much higher rate and at 300°C it reached the lowest value of all three specimens tested. The

analysis of complete stress-strain curves showed that at low temperatures the alloy exhibited a limited ductility.

Enhanced ductility exceeding 40% was observed at elevated temperatures (> 200°C). Both the yield stress and the ultimate strength decreased with increasing temperature. However, only incomplete tests could have been performed on specimens after ECAP. Due to limited dimensions of the test billets (15 mm in height) the tests had to be stopped before the ultimate stress was reached (usually at the specimen height of 3-5 mm) and no data on the temperature dependence of the ultimate strength and the ductility are therefore available. AE measurements during compression tests were performed at various temperatures and in as cast and two ECAPed specimens.

Fig. 10 shows the compression test results for squeeze-cast AZ31 at various temperatures (room temperature, 200°C and 300°C) together with the detected AE recordings. The yield strength decreases while the ductility increases with temperature, which is not surprising. The AE count rates exhibit a characteristic maximum related to the macroscopic yield point, which is followed by an AE activity with slowly decreasing count rate values. This behaviour lasts until fracture. The AE signals are very strong for all three conditions; they even rise at elevated temperatures, being strongest at 200°C. A similar observation was made by (Máthis et al., 2004) for an AM 50 alloy, where an even more pronounced effect was seen.

Fig. 11 shows the results for ECAP deformed squeeze-cast AZ31 tested in compression at room temperature. As expected, the yield strength is seen to increase significantly already after a single ECAP pass. Further increase was observed after four passes (4 P). The shape of the AE count rate versus strain curves is very similar to that for the squeeze-cast alloy (0 P). The AE activity of the single pass (1 P) specimen at room temperature is almost identical to that of the non-ECAPed AZ31 suggesting that the mechanisms responsible for AE are the same in these two conditions. This is different for the 4 P specimen, which already had a pronounced ultra-fine grained structure. The AE activity is about a factor of 10 lower than in the previous case, which indicates a significant influence of the microstructure on the AE mechanisms.

The AE behaviour of the ECAPed specimens at 200°C is presented in Fig. 12. For 1 P specimen the same effect can be seen as the one observed for the non-ECAPed specimens. The AE activity sustains up to significantly higher strains than in the case of room temperature compression. This again confirms the similarity of the AE behaviour of non-ECAPed and 1 P specimens. For the 4 P specimen only a very weak AE signal could be detected at 200°C. This indicates that a change in the deformation processes has taken place.

The compression tests at 200°C on ECAPed specimens do not show any surprising results: a significant decrease in yield strength was observed for 4 P specimen, which was less pronounced for 1 P specimen.

The AE behaviour of the ECAPed specimens at 200°C is presented in Fig. 12. For 1 P specimen the same effect can be seen as the one observed for the non-ECAPed specimens. The AE activity sustains up to significantly higher strains than in the case of room temperature compression. This again confirms the similarity of the AE behaviour of non-ECAPed and 1 P specimens. For the 4 P specimen only a very weak AE signal could be detected at 200°C. This indicates that a change in the deformation processes has taken place.

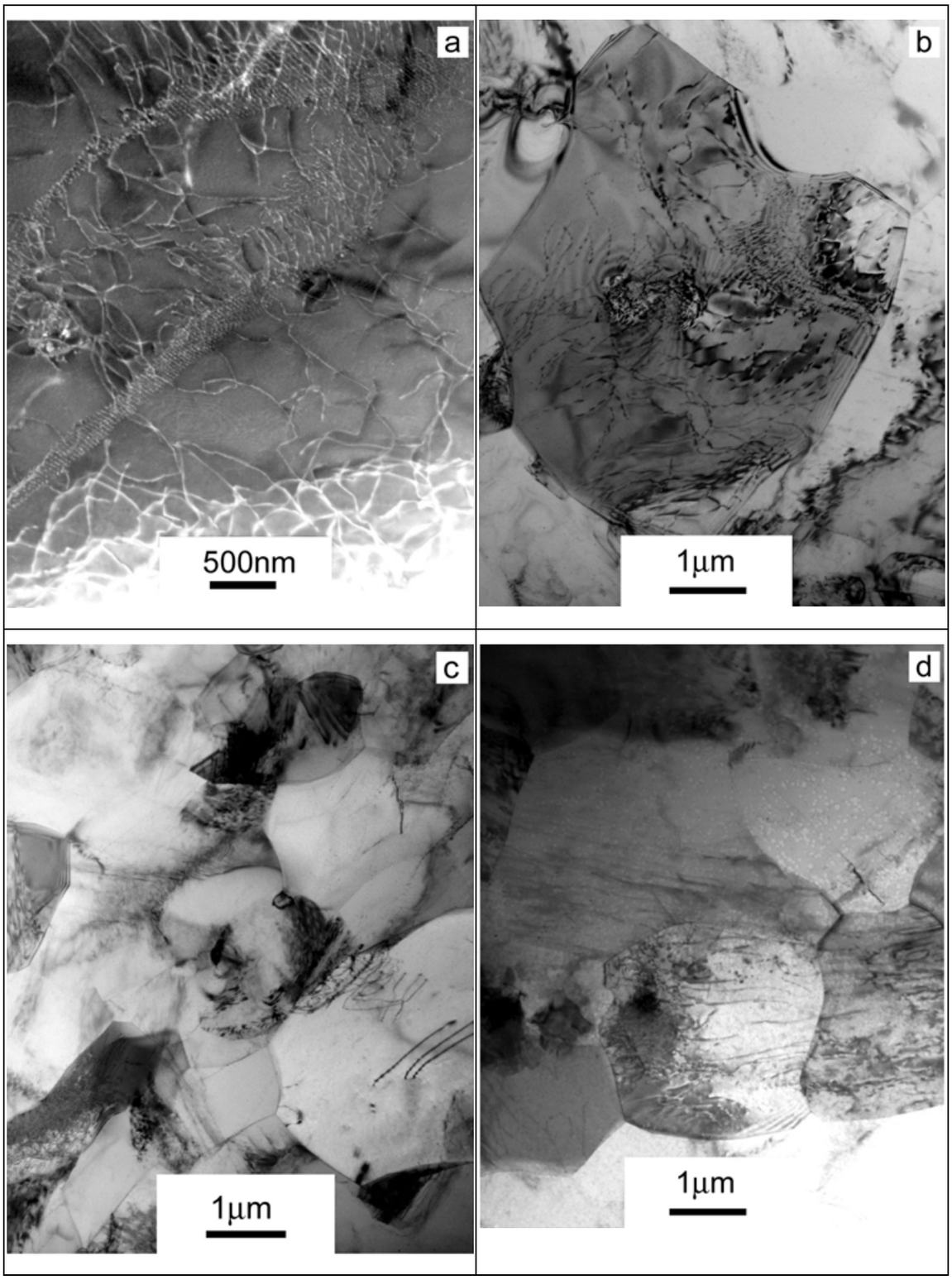

Fig. 8. The microstructure changes in the deformed specimen at 300°C, a) 1 pass, X plane, b) 4 passes, X plane, c) 1 pass, Y plane, d) 4 passes Y plane

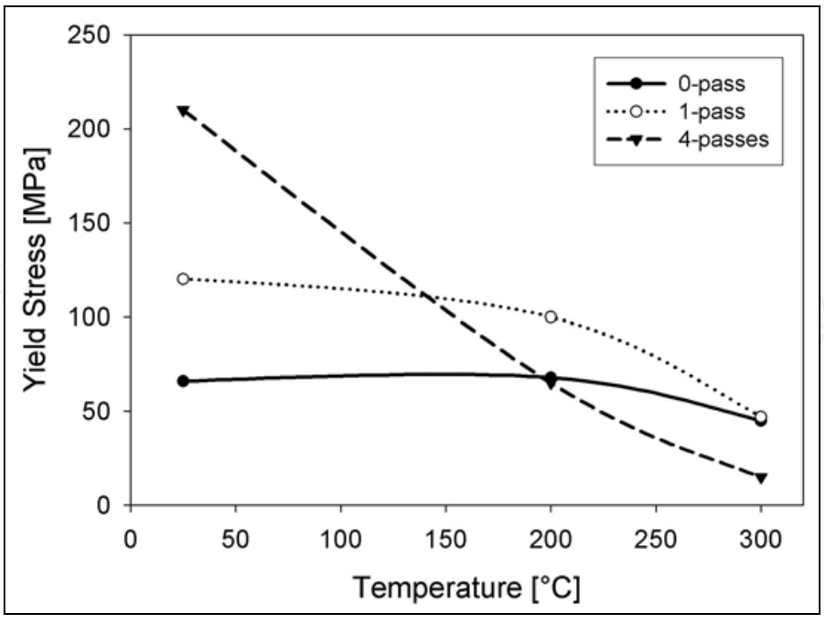

Fig. 9. The yield stress of the non-deformed AZ31 and AZ31 after ECAP at different temperatures

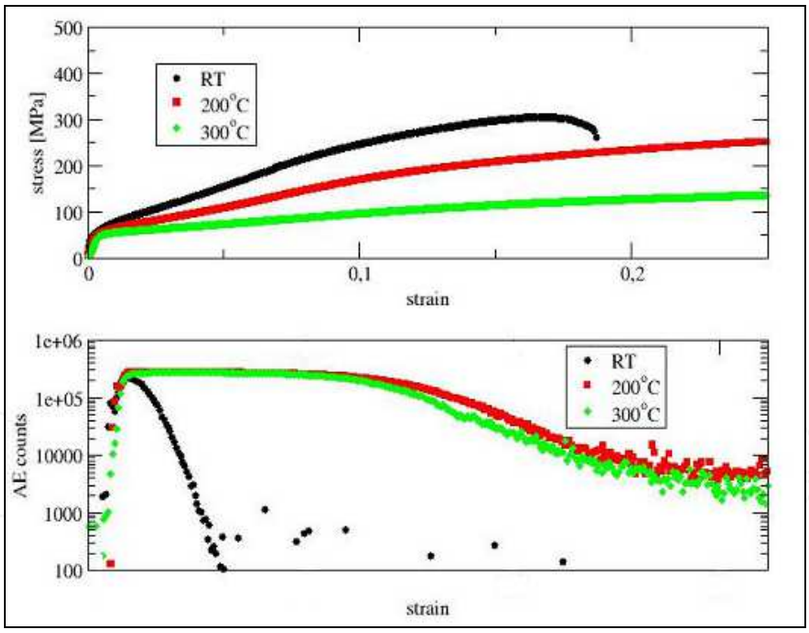

Fig. 10. Compressive true stress–true strain curves vis-à-vis AE at 3 different temperatures for as-cast AZ31. The scale of strain is the same in both figures

The compression tests at 200°C on ECAPed specimens do not show any surprising results: a significant decrease in yield strength was observed for 4 P specimen, which was less pronounced for 1 P specimen.

The AE behaviour of the ECAP processed specimens under subsequent compression at 300°C is shown in Fig. 13. For 1 P specimen, a strong decrease in AE counts was observed

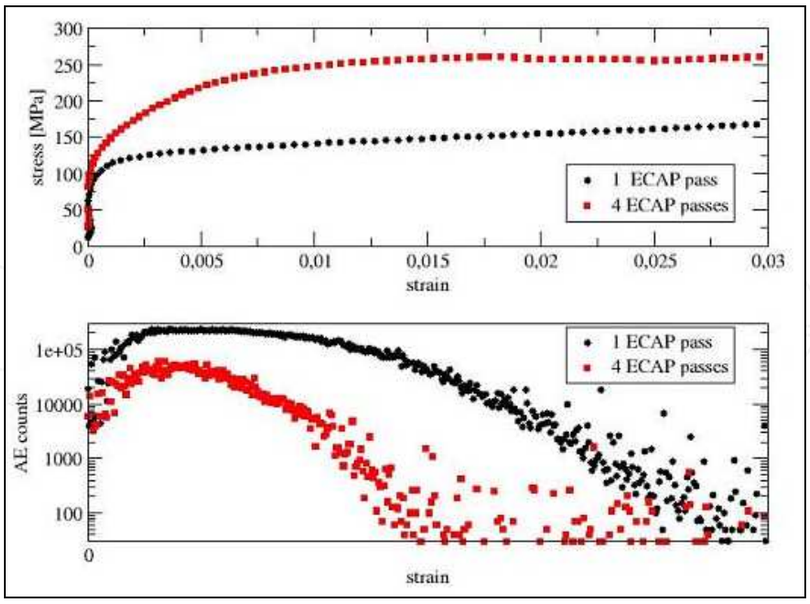

Fig. 11. Compressive true stress–true strain curves vis-à-vis AE at room temperature for ECAP processed specimens (1 and 4P). The scale of strain is the same in both figures

for larger strains, as distinct from the behaviour found for the non-ECAPed deformed material. The 4 P specimen exhibits almost no AE, which confirms the tendency already observed in compression tests at 200°C. With further increase of temperature, at 300°C, the yield strength dropped to very low values around 50MPa (1 P) and 15MPa (4 P).

AE signals correlate well with microstructure processes operating during ECAP straining and/or following compression deformation.

At room temperature compression, the AE is most likely caused by dislocation avalanches produced by dislocation slip as well as twinning (Heiple & Carpenter, 1987). The AE peak at the yield point can be attributed to massive dislocation multiplication accompanied with twinning. With increasing strain the multiplication of forest dislocations decreases the AE count rate by reducing the flight distance of moving dislocations. During deformation of the coarse grained specimens persisting twinning is commonly observed (Barnett et al., 2004). That is why the decrease of the AE activity in AZ31 is less pronounced than, e.g., in Al alloys (Heiple & Carpenter, 1987). The explanation of the observed increase of the AE count rate with increasing temperature which was also reported in other alloys (e.g., Máthis et al., 2004) is still ambiguous. One of possible interpretations of this effect is the interplay between twinning and dislocation glide under conditions of enhanced recovery. This may explain the AE behaviour observed at 200°C and 300°C. The slightly lower AE at 300°C could be a result of a less pronounced effect of twinning at this high temperature, while collective dislocation motion is still operative (Máthis et al., 2004). Starting at about 200°C dislocation motion is also activated on non-basal slip planes, which is further facilitated at 300°C (Polmear, 1992). Therefore, twinning becomes less important and, consequently, the overall AE activity is reduced.

In 1 P ECAPed specimen the AE curves were almost identical with those of the non-ECAPed material. Our TEM observations may contribute to the explanation of this behaviour. In 1P ECAPed specimen a significant portion of the original coarse grain microstructure was still

retained. Therefore the AE behaviour of 1 P specimen showed similarity with the non-ECAPed material. In 4 P specimen a new grain structure was observed by TEM. In particular, in 4 P specimen deformed at 200°C almost fully recrystallized structure with an average grain size of about 800 nm was found. The fine grain structure leads to a smaller mean free path of gliding dislocations. Moreover, it suppresses the propensity for twinning, which reduces the AE count rate (Kiesewetter & Schiller, 1976). All this can explain the generally lower AE activity observed in specimens after 4 ECAP passes.

At 200°C compression, a significantly (about one order) reduced AE activity at higher strains in 1 P ECAPed specimen as compared to the non-ECAPed specimen is probably caused by reduced contribution of collective dislocation motion and/or twinning In 4 P specimen only a very low AE signal was detected which further support the assumption of reduced dislocation motion or twinning. As the 4 P pass material has a recrystallized ultra-fine grained structure, dynamic recrystallization must have occurred during subsequent compression testing. Obviously, the recrystallization reduces the amount of twinning and collective dislocation motion (as manifested in reduced AE activity), most likely owing to elimination of stress concentration sites necessary to initiate the above processes.

At 300°C compression, the collective dislocation glide in 1 P ECAPed specimens concurs with dynamic recrystallization taking place during compression testing. TEM investigations revealed an inhomogeneous structure, which contains recrystallized grains of 1μm in diameter in one direction co-existing with a deformed microstructure containing a high density of heterogeneously distributed dislocations. No signs of twinning were seen in the TEM pictures. This is in agreement with a strongly reduced AE activity measured in these specimens. The structure of the 4 P ECAPed specimens after compression tests showed a fully recrystallized microstructure with a grain size ranging from 1 μm to 10μm. Again, owing to the initial ultra-fine grained recrystallized structure that existed prior to the compression test, no AE activity whatsoever was detected.

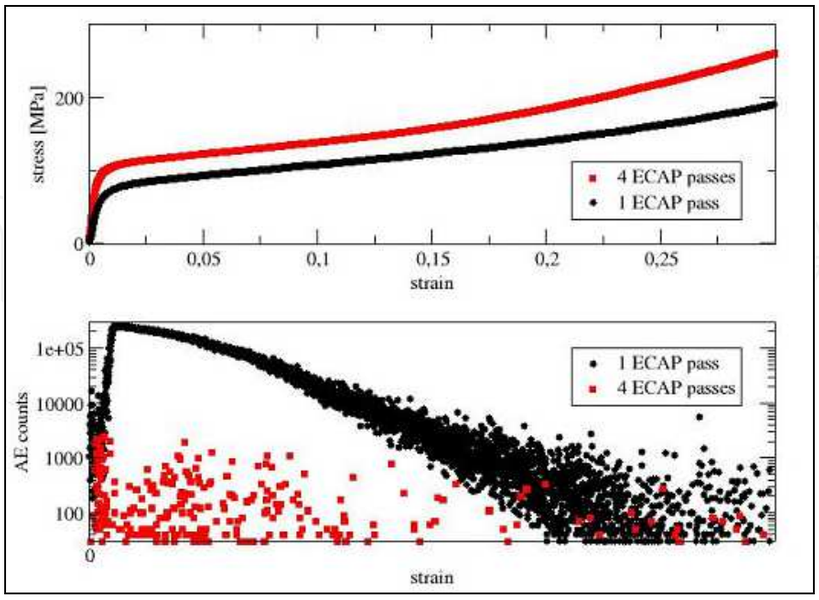

Fig. 12. Compressive true stress–true strain curves vis-à-vis AE at 200°C for ECAPed specimens. The scale of strain is the same in both figures.

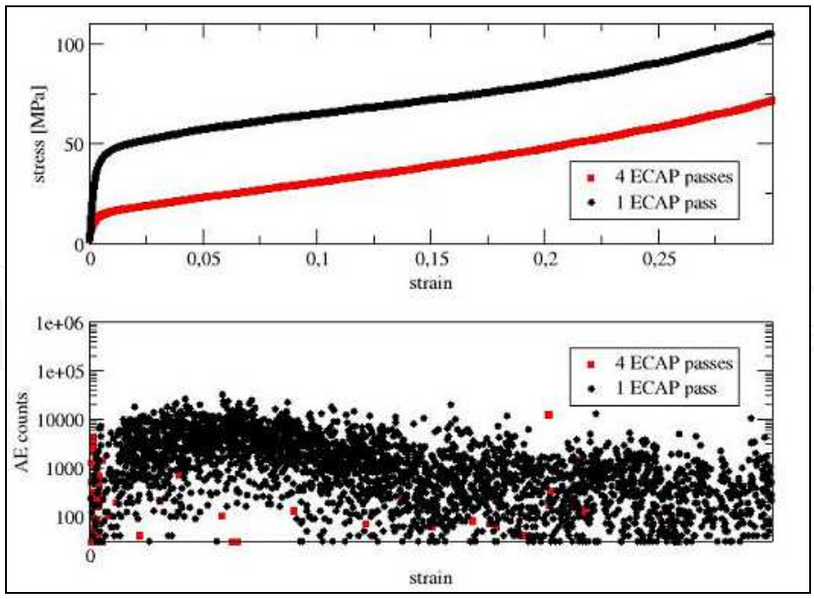

Fig. 13. Compressive true stress–true strain curves vis-à-vis AE at 300°C for ECAPed specimens. The scale of strain is the same in both figures.

3.2.2 Microstructure and texture evolution

As cast AZ31 alloy was processed by equal channel angular pressing (ECAP) at 180°C following route B_c resulting in a maximum equivalent strain of 12 (1, 2, 4, 8 and 12 passes). Prior to ECAP, the specimens were extruded at T = 350°C with extrusion ratio ER = 22. The texture of the extruded and the ECAPed samples was analyzed by the electron backscatter diffraction (EBSD). Samples for EBSD measurements were cut from ECAPed billets from the plane perpendicular to the pressing direction (plane X). EBSD scans were carried out at the mid-part of the cross-section of each billet.

The microstructure of the initial extruded bar (0P) shown in Fig. 14 consists of large grains of 50 ~ 100μm and relatively fine grains of 2 ~ 5μm around the large ones. Most grains have their crystallographic c-axis perpendicular to the extrusion direction (ED), i.e. <10-10> axes parallel to the ED, which is typically found after extrusion of Mg alloys.

Fig. 15 presents the microstructure and texture of sample after 1 ECAP pass (1P). Sample coordinate system, i.e. X–Y–Z directions, which is used for representing the textures are illustrated in Fig. 15d. As shown in Fig. 15a, the bimodal distribution of grain sizes is still observed in the 1P sample. A new texture component, which corresponds to the basal poles rotated about 40° from the initial orientation towards the pressing direction, is visible in the 1P sample, Fig. 15b. This mechanism caused by the shear strain imposed by ECAP was also reported by other authors (Estrin, 2008). However, the mentioned orientation change is observed mainly in large grains (grain size of 10 μm). Figure 15c presents the (0001) pole figure of grains smaller than 3 μm in the 1P sample. The intensity of the tilted basal poles is rather weak compared to the pole figure constructed using all grains. Moreover, the small grains (< 3 μm) with the tilted basal pole are found mainly in neighbouring areas around large grains. These results regarding distinct textures depending on the grain sizes indicate that the shear strain by the first ECAP pass is mainly accommodated within the large grains. It corresponds well to the fact that larger grains are deformed by lower energy comparing to

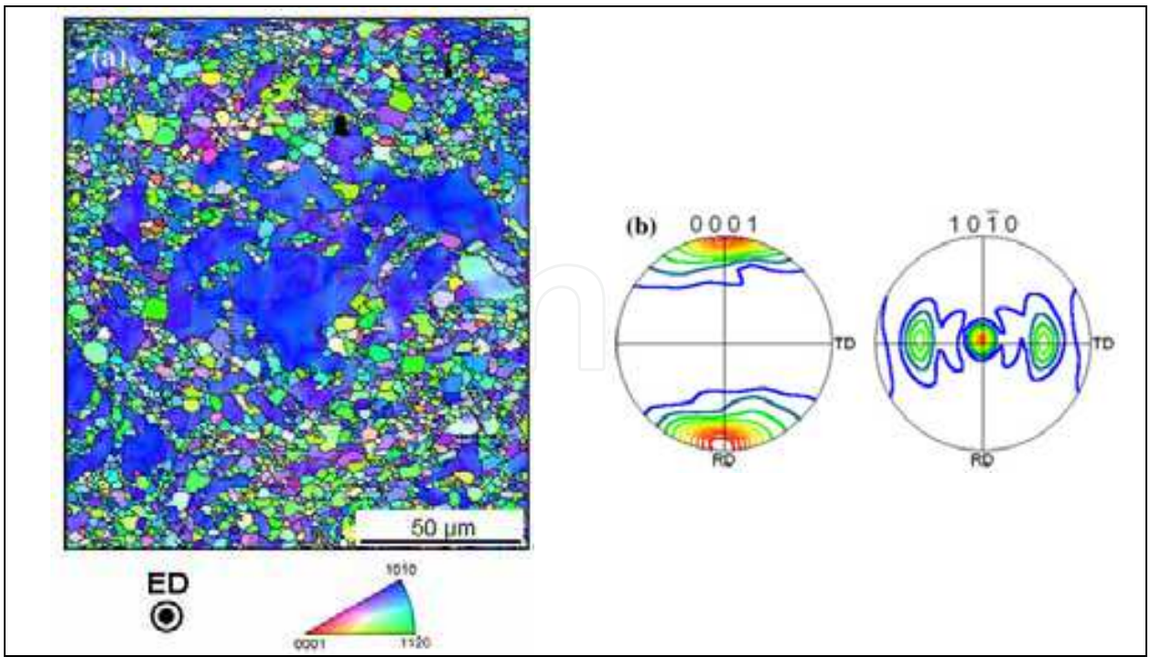

Fig. 14. (a) - EBSD orientation map, (b) - recalculated pole figures of the extruded bar (0P), measured at the cross-section transverse to the extrusion direction (contour level = 1, 2, ...10)

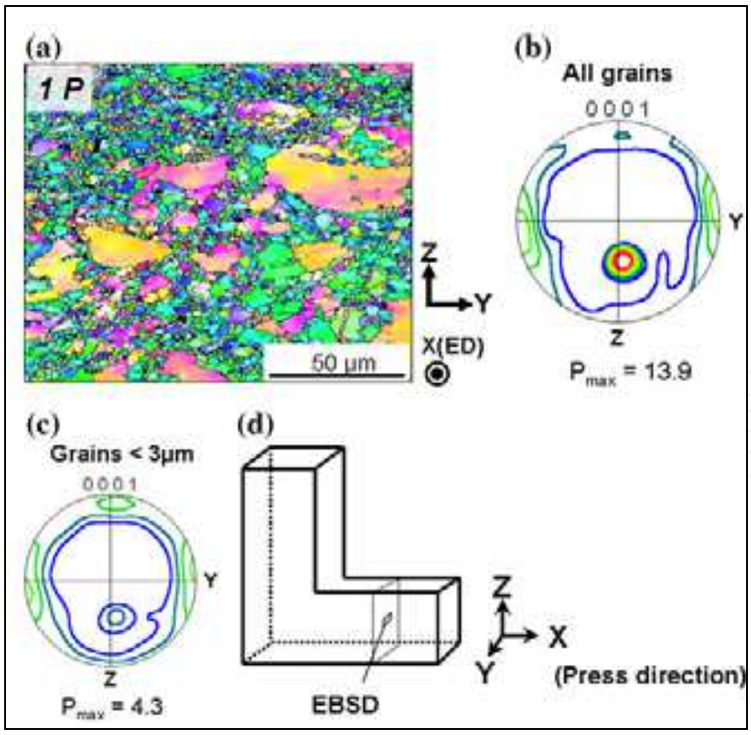

Fig. 15. (a) - EBSD orientation map of the sample after 1 ECAP pass, (b) - (0001) pole figure calculated using all grains, (c) - (0001) pole figure of grains smaller than 3 µm and (d) - the scheme of the geometry of specimens for EBSD measurements (contour level = 1, 2, … 10)

the small grains, e.g. Hall–Petch relation. The discontinuity of material flow caused by the inhomogeneous deformation seems to be compensated by the occurrence of the dynamic recrystallisation in the vicinity of grain boundaries of large grains, such that the sample could be deformed without failure. Microstructural features of the sample after 2 ECAP passes are very similar to those after 1 ECAP pass, i.e. the bimodal distribution of grain sizes and the orientation change in large grains remain almost unchanged.

The amount of large grains decreases significantly after 4 ECAP passes (4P), and their size becomes smaller when compared to the initial and the 1P samples. Moreover, fine grains were observed mainly near grain boundaries of large grains. It indicates that the refinement of large grains occurs gradually with increasing strain due to ECAP by dynamic rotation mechanism suggested by (Ion, et al., 1982). Differently to the 1P sample, the fine grains (<3 μm) have mainly the orientation of the rotated basal poles in the 4P sample, Fig. 16a. Comparing pole figures evaluated from the whole area of the EBSD measurement to that from fine grains (<3 μm) Fig. 16a and b, indicates unambiguously that the texture heterogeneity depending on the grain size disappears after 4 ECAP passes.

The 12P sample, Fig. 17, shows the homogeneous distribution of fine almost equiaxed grains, i.e. no large grains are visible. Fig. 17a shows grain agglomerates, having different colours, distributed along a diagonal line. This indicates the heterogeneity in texture depending on the

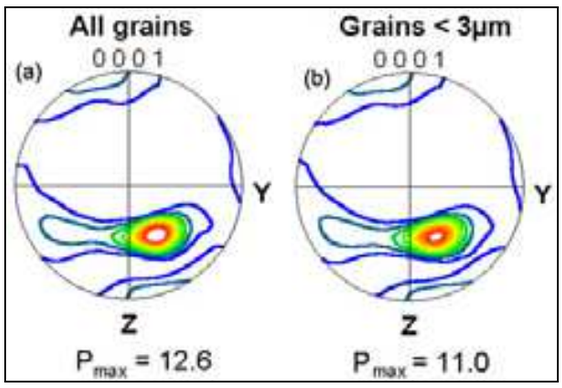

Fig. 16. (a) - (0001) pole figure of all grains and (b) - grains smaller than 3 μm (contour level = 1, 2, … 10)

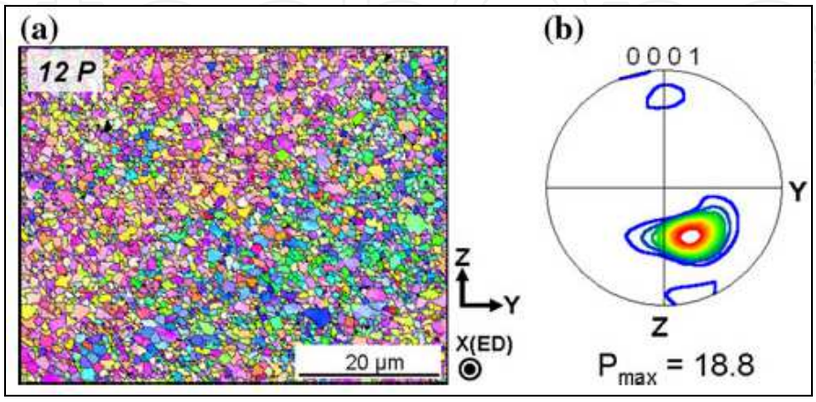

Fig. 17. (a) - EBSD orientation map and (b) - (0001) pole figure of the sample after 12 ECAP passes (contour level = 1, 2, … 15)

locations. This texture inhomogeneity can be understood as a result of non-uniform deformation along the ECAP billet after multiple passes (Agnew et al, 2005) Though the heterogeneous texture is visible, the fraction of the grains relating to the inhomogeneity is small such that the main texture component is found at the rotated basal pole, Fig. 17b.

3.3 Mechanical and fatigue properties of cast and wrought AZ31 alloy

Sufficient fatigue resistance is an important requirement on engineering materials used for components subjected to cyclic loading. The demand for improving the efficiency of automotive vehicles, particularly by weight reduction, results in tougher requirements on fatigue resistance of Mg alloys as candidate materials for automotive parts. To that end, a better knowledge of fatigue behavior and damage processes in relation to the microstructure of Mg alloys is necessary. Microstructure and mechanical properties strongly depend on the method of processing.

AZ31 alloy is often produced as a high pressure cast material, because it exhibits excellent castability. Squeeze casting (SC) consisting of two casting steps is one of the most frequently applied procedures. Wrought AZ31 alloy have had a much more limited use than the high-pressure die castings. To date, the knowledge of the fatigue behavior of wrought alloys is surprisingly limited.

Conventional AZ31 alloy was prepared by three different processing techniques: squeeze casting at 200°C employing a two step loading process, hot rolling (HR) at 370°C and 4 pass route B_C ECAP pressing of the HR material at 200°C. The microstructure of these materials was investigated by (Zúberová et al., 2007). SC alloy has a typical dendritic structure comprising large grains of 450 μm. HR material exhibited a homogeneous structure with grains in the range of 3 to 20 μm while ECAP specimen consisted of almost equiaxed grain with average size of 1 to 2 μm.

A comparison of the tensile stress-strain curves for all three materials is shown in Figure 18 and summarized in Table 1.

As expected the ductility was found to increase with grain refinement (from SC over HR to ECAP). The improved ductility of ECAP specimen with respect to HR one may be explained by texture development that occurs during ECAP (see the section 3.2.2). For Mg alloys, basal planes tend to lie parallel to the extrusion direction after extrusion, indicating that slip on the basal plane becomes difficult and the strength increases due to limited nonbasal slip activity (Kim et al, 2005). The enhancement of tensile ductility after ECAP could be a result of large strain hardening after yielding, in addition to the aforementioned texture effect.

Enhanced hardening may be attributed to the activation of two or more slip planes as a consequence of rotation of slip planes during ECAP (Kim et al, 2005).

The experimentally determined fatigue life of squeeze cast, hot-rolled, and ECAP-processed AZ31 alloy is shown in Figure 19. It can be seen that there is a strong influence of the production procedure on the fatigue properties. The SC material exhibits the lowest fatigue strength of approximately 40 MPa. HR improves the fatigue life substantially, while ECAP exhibits slightly worse fatigue behaviour. However, in the high-cycle region both HR and ECAP exhibit the same fatigue strength of 95 MPa. An increase of fatigue strength is very often related to grain size reduction. The explanation can be sought in inhibited crack initiation and in an increase of the number of barriers to early crack propagation. Smaller grains also tend to inhibit dislocation motion. Our finding that severe plastic deformation of

hot-rolled AZ31 by ECAP does not result in any improvement of fatigue life suggests that a reduction in strength associated with the texture effects (as seen for monotonic deformation (Somekawa & Mukai, 2006) may counterbalance concurrent strengthening due to grain refinement. ECAP is also known to change the character of grain boundaries which may also affect the tensile strength.

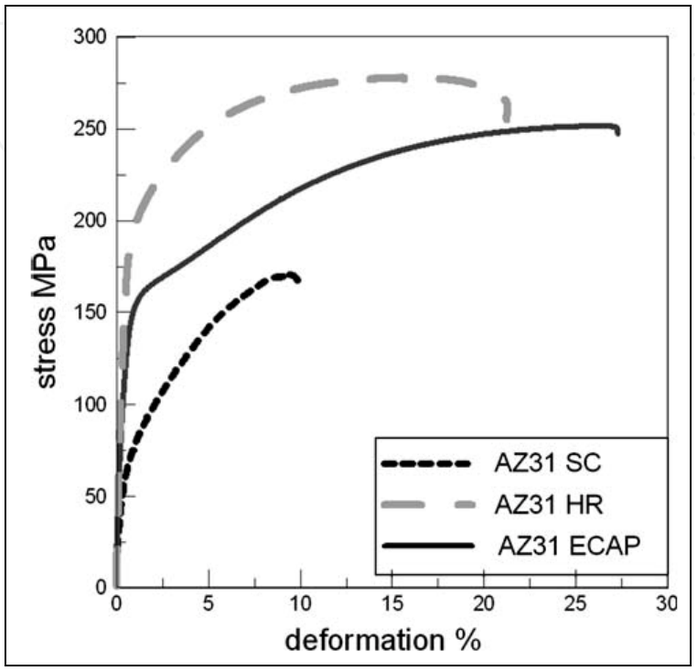

Fig. 18. Tensile curves of AZ31 alloy in SC, HR and ECAP condition

AZ31	YS (MPa)	UTS (MPa)	Ductility (%)	Endurance limit (MPa)
SC	50	170	10	40
HR	175	277	21	95
ECAP	175	251	27	95

Table 1. Tensile and fatigue properties of AZ31 alloy

4. Summary and conclusions

4.1 Hot rolled AZ31

- The ductility of hot-rolled AZ31 alloy increases significantly with the deformation temperature and with the preheating temperature.
- Serrated yielding (PLC effect) was observed in a hot-rolled AZ31 alloy at all deformation temperatures and strain rates.
- Twinning characterized by a compound mode with differently oriented twins intersecting each other is the dominant mechanism in the initial stage of deformation.

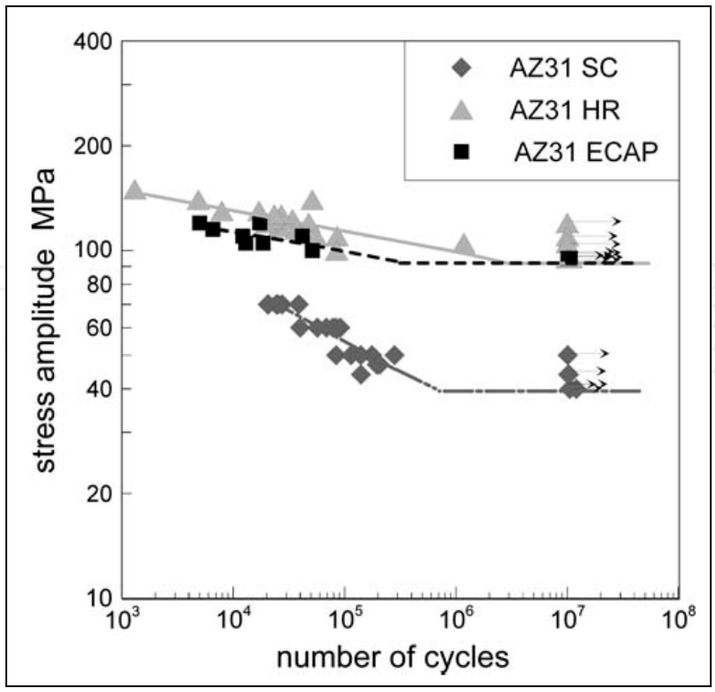

Fig. 19. Comparison of fatigue life in SC, HR and ECAP conditions

- Total AE activity is a result of interplay of different effects, mainly twinning and PLC effect. The challenge for the future is to separate the respective AE bursts.
- Strong anisotropy of mechanical properties was found in the extruded alloy. Much weaker anisotropy was found in the cast alloy. After rolling the anisotropy was smeared out.
- The temperature of 350°C seems to be the optimum preheating temperature for attaining the best mechanical properties of hot rolled sheets both from the extruded and the cast material.
- Significant strain hardening due to twinning occurs during room temperature deformation of hot-rolled specimens.
- Significant grain refinement was found after rolling. The temperature of preheating influences the final rolled structure, which tends to coarsen with increasing T.
- Numerous cracks were observed in the cast alloy after rolling due to extensive porosity.
- dynamic recrystallisation occurs during rolling. The rate of dynamic recrystallisation is enhanced by the temperature of preheating.

4.2 Ultrafine-grained AZ31 processed by ECAP

a) Mechanical properties vis-à-vis AE

- As-cast AZ31 specimens exhibited strong AE at all testing temperatures, which can be explained as a result of collective dislocation motion and twinning.
- At room temperature and 200°C, a single pass ECAP processed specimen exhibited AE behaviour similar to that of the as-cast material. This can be rationalized as a result of an inhomogeneous microstructure containing residual coarse grained regions co-existing with regions of heavily deformed material with a high dislocation density.

- At 300°C the AE was significantly reduced due to the occurrence of dynamic recrystallization.
- Four pass ECAP processed specimens, with their ECAP induced recrystallized structure with a grain size of 800 nm, show a reduced AE activity already at room temperature. As this material exhibited dynamic recrystallization during compression tests at 200°C and 300°C, AE signals under these conditions were very weak if any.
- The average size of dynamically recrystallized grains increases with increasing strain imposed by ECAP.
- Dynamic recrystallization occurs during the deformation of ECAPed specimens at high temperatures.

b) Microstructure and texture evolution with strain due to ECAP

- The first pass (1P) of ECAP results in the formation of a new texture component inclined by about 40° relatively to the initial texture.
- The bimodal character of the microstructure remains unchanged up to 4P of ECAP.
- Further ECAP pressing (8 and 12P) results in a completely refined microstructure.
- The refinement of large grains occurs gradually with increasing ECAP passes by dynamic rotation recrystallization mechanism.
- The grain size was reduced by a factor of about 100–200 through ECAP processing.

4.3 Mechanical and fatigue properties of cast and wrought AZ31

- Mechanical properties of cast material are inferior to those of wrought alloy.
- Hot rolled and ECAPed alloy exhibited substantially higher ultimate tensile strength, fatigue life and endurance limit than cast alloy.
- Subsequent ECAP processing does not result in further improvement of fatigue properties of hot rolled alloy despite the marked grain refinement it produces, most probably due to the texture effects and a change in the character of grain boundaries.
- Control of complex interplay of all these factors poses a challenge to ''grain boundary engineering'' aimed at optimization of the alloy properties.

5. Acknowledgement

This work was financially supported through the research program MSM 0021620834 of Ministry of Education of the Czech Republic.

6. References

Agnew, S.R., Lillo, T.M., Macheret, J., Stoica, G.M., Chen, L., Lu, Y., Fielden, D., Liaw, P.K. (2001). Assessment of equal channel angular extrusion processing of magnesium alloys, *Proceedings of the Magnesium Technology Symposium*, pp. 243–247, New Orleans, Louisiana, February 11–15.

Agnew, S.R., Mehrotra, P., Lillo, T.M., Stoica, G.M., Liaw, P.K. (2005). Crystalographic texture evolution of three wrought magnesium alloys during equal channel angular extrusion, *Mater Sci Eng.*, A408, 72-78.

ASTM (1994). *Test Methods of Tension Testing Wrought and Cast Aluminium-and Magnesium-Alloy Products. Annual Book of ASTM Standards.* ASTM B 557-94 (1994). West Conshohocken, PA, ASTM International, vol. 02.02.

Barnett, M.R. , Keshavarz, Z., Beer, A.G., Atwell, D. (2004). Influence of grain size on the compressive deformation of wrought Mg-3Al-1Zn, *Acta Mater.*, 52, 5093–5103.

Bohlen, J., Chmelík, F., Dobroň, P., Kaiser, F., Letzig, D., Lukáč, P., Kainer, K.U. (2004). Orientation effects on acoustic emission during tensile deformation of hot rolled magnesium alloy AZ31, *J Alloys Compd.*, 378, 207–213.

Botten, R., Wu, X., Hu, D., Loretto, M.H. (2001). The significance of acoustic emission during stressing of TiAl-based alloys. Part I: Detection of cracking during loading up in tension, *Acta Mater.*,49, 1687-1691.

Cáceres, C.H., Griffiths, J.R., Davidson, C.J., Newton, C.L. (2002). Effects of solidification rate and ageing on the microstructure and mechanical properties of AZ91 alloy, *Mater. Sci. Eng.,A 325*, 344–355.

Chmelík, F., Ziegenbein, A., Neuhäuser, H., Lukáč, P. (2002). Investigating the Portevin–Le Châtelier effect by the acoustic emission and laser extensometry techniques, *Mater. Sci. Eng,*. A 324, 200–207.

Corby, C., Cáceres, C.H., Lukáč, P. (2004). Serrated flow in magnesium alloy AZ91*Mater. Sci. Eng.* A387-389, 22-24.

Emley, E.F. (1996). *Principles of Magnesium Technology*, Pergamon Press, 978-0849355547, London.

Estrin, Y., Yi, S., Brokmeier, H.G., Zúberová, Z., Yoon, S.C., Kim, H.S., Hellmig, R.J. (2008). Microstructure, texture and mechanical properties of the magnesium alloy AZ31, *Int. J Mater. Res.*, 99, 50-55

Friesel, M., Carpenter, S.H. (1984). Acoustic emision investigation during the deformation of pure Mg and AZ31B alloy. *J Acoustic Emission*, 3, 11-17.

Heiple, C.R., Carpenter, S.H. (1987). Acoustic emission produced by deformation of metals and alloys, *J Acoustic Emission*, 6, 215-237.

Ion, S.E., Humphreys, F.J., White, S.H. (1982). Dynamic recrystallization and the development of microstructure during the high temperature deformation of magnesium, *Acta Mater.*, 30, 1909-1919.

Ishikawa, K., Watanabe, H., Mukai, T. (2005). High temperature compressive properties over a wide range of strain rates in an AZ31 magnesium alloy, *J Mater. Sci.*, 40, 1577–1582.

Kaiser, F., Letzig, D., Bohlen, J., Styczynski, A., Hartig, Ch., Kainer, K.U. (2003). Anisotropic Properties of Magnesium Sheet AZ31, *Mater. Sci. Forum*, 419–422, 315-320.

Kaiser, J. (1953). Erkenntnisse und Folgerungen aus der Messung von Geräuschen bei Zugbeanspruchung von Metallischen Werkstoffen, *Arch. Eisenhüttenwes., 24, 43-45.*

Kamado, S., Ashie, T., Yamada, H., Sanbun, K., Kojima, Y. (2000). Improvement of tensile properties of wrought magnesium alloys by grain refining, *Mater. Sci. Forum*, 350–351, 65–72.

Kiesewetter, N., Schiller, P. (1976). The acoustic emission from moving dislocations in aluminium, *Phys. Status Solidi*, (a) 38, 569–576.

Kim, H.K., Lee, Y.I., Chung, C.S. (2005), Fatigue properties of a fine-grained magnesium alloy produced by equal channel angular pressing, *Scripta Mater.*, 52, 473-77.

Kim, W.J., Hong, S.I., Kim, Y.S., Min, S.H., Jeong, H.T., Lee, J.D. (2003). Texture development and its effect on mechanical properties of an AZ61 Mg alloy fabricated by equal channel angular pressing, *Acta Mater.*, 51, 3293-3307.

Král, R., Dobroň, P., Chmelík, F., Koula, V., Rydlo, M., Janeček, M. (2007). A qualitatively new approach to acoustic emission measurements and its application to pure aluminium and Mg-Al alloys, *Kovove Mater.*, 45, 159-163.

Lamark, T.T., Chmelík, F., Estrin, Y., Lukáč P. (2004). Cyclic deformation of a magnesium alloy investigated by acoustic emission, *J Alloys & Comp.*, 378, 202-206.

Mabuchi, M., Iwasaki, H., Yanase, K., Higashi, K. (1997), Low temperature superplasticity in an AZ91 magnesium alloy processed by ECAE, *Scripta Mater.*, 36, 681-686.

Máthis, K., F. Chmelík, F., Trojanová, Z., Lukáč, P., Lendvai, J. (2004). Investigation of some magnesium alloys by use of acoustic emission technique, *Mater. Sci. Eng.*, A 387–389, 331–335.

Máthis, K., Chmelík, F., Janeček, M., Hadzima, B., Trojanová, Z., Lukáč, P. (2006). Investigating deformation processes in AM60 magnesium alloy using the acoustic emission technique, *Acta Mater.*, 54, 5361.

Matsubara, K., Miyahara, Y., Horita, Z., Langdon, T.G. (2003). Developing superplasticity in a magnesium alloy through a combination of extrusion and ECAP, *Acta Mater.*, 51, 3073-3084.

Mukai, T., Yamanoi, M., Watanabe, H., Higashi, K. (2001). Ductility enhancement in AZ31 magnesium alloy by controlling its grain structure, *Scripta Mater.*, 45, 89–94.

Polmear, I.J. (1992), *Magnesium Alloys and Their Applications*, Mordike, B.L. , F. Hehmann F. (Eds.), , DGM, Oberursel, pp. 201

Richeton, T., Dobroň, P., Chmelík, F., Weiss, J., Louchet, F. (2006). On the critical character of plasticity in metallic single crystals, *Mater. Sci. Eng.*, A424, 190-195.

Segal, V.M. (1995). Materials processing by simple shear, *Mater. Sci. Eng.*, A197, 157.

Tan, J.C, Tan, M.J. (2002). Superplasticity in a rolled Mg-3Al-Zn alloy by two-stage deformation method, *Scripta Mater.*, 47, 101–106.

Somekawa, H., Mukai, T. (2006). Fracture thoughness in Mg-Al-Zn alloy processed by equal channel angular extrusion, *Scripta Mater.*, 54, 633-638.

Trojanová, Z., Cáceres, C. (2007). On the strain to the onset of serrated flow in AZ91 alloy, *Scripta Mater.*, 56, 793-796.

Valiev, R.Z., Islamgaliev R.K., Alexandrov, I.V. (2000), Bulk Nanostructured Materials from Severe Plastic Deformation, *Prog. Mater. Sci.*, 45, 103-189.

Vinogradov, A., Merson, D.,L., Patlan, V., Hashimoto, S. (2003). On the mechanism of unstable plastic flow in an austenitic FeMnC TWIP steel, *Mater. Sci. Eng.*, A341, 57-73.

Watanabe, H., Mukai, T., Ishikawa, K., Higashi, K. (2003). Superplastic behaviour of an ECAE processed ZK60 magnesium alloy, *Mater. Sci. Forum*, 419-422, 557-562.

Yin, D.L., Zhang, K.F., Wang, G.F., Han, W.B. (2005). Warm deformation behaviour of hot-rolled AZ31 Mg alloy, *Mater. Sci. Eng.*, A392, 320-325.

Yoshida, Y. , Arai, K., Itoh, S., Kamado, S., Kojima, Y. (2004). Superplastic deformation of AZ61 magnesium alloy having fine grains, *Mater. Trans.*, 45, 2537-2541.

Zhang, P., Watzinger, B., Kong, P.Q., Blum, W. (2000). Microstructural evolution during creep of Mg-Al alloy AZ91hp, *Key Eng. Mater.* 171–174, 609–616.

Zúberová, Z., Estrin, Y., Lamark, T.T., Janeček, M., Hellmig, R.J., Krieger, M. (2007), Effect of equal channel angular pressing on the deformation behaviour of magnesium alloy AZ31 under uniaxial compression, *Jour. Mat. Proc. Technol.*, 184, 294-299.

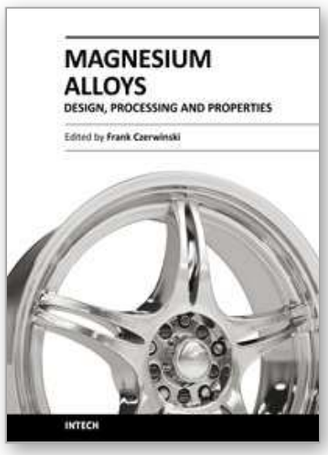

Magnesium Alloys - Design, Processing and Properties

Edited by Frank Czerwinski

ISBN 978-953-307-520-4
Hard cover, 526 pages
Publisher InTech
Published online 14, January, 2011
Published in print edition January, 2011

Scientists and engineers for decades searched to utilize magnesium, known of its low density, for light-weighting in many industrial sectors. This book provides a broad review of recent global developments in theory and practice of modern magnesium alloys. It covers fundamental aspects of alloy strengthening, recrystallization, details of microstructure and a unique role of grain refinement. The theory is linked with elements of alloy design and specific properties, including fatigue and creep resistance. Also technologies of alloy formation and processing, such as sheet rolling, semi-solid forming, welding and joining are considered. An opportunity of creation the metal matrix composite based on magnesium matrix is described along with carbon nanotubes as an effective reinforcement. A mixture of science and technology makes this book very useful for professionals from academia and industry.

InTech Europe
University Campus STeP Ri
Slavka Krautzeka 83/A
51000 Rijeka, Croatia
Phone: +385 (51) 770 447
Fax: +385 (51) 686 166
www.intechopen.com

InTech China
Unit 405, Office Block, Hotel Equatorial Shanghai
No.65, Yan An Road (West), Shanghai, 200040, China
中国上海市延安西路65号上海国际贵都大饭店办公楼405单元
Phone: +86-21-62489820
Fax: +86-21-62489821

IntechOpen